Influence of shear flow on the formation of rings in wormlike micelles: A nonequilibrium molecular dynamics study

J. T. Padding[1,2,*] and E. S. Boek[1,†]
[1]*Schlumberger Cambridge Research, High Cross, Madingley Road, Cambridge CB3 0EL, United Kingdom*
[2]*Department of Chemistry, University of Cambridge, Lensfield Road, Cambridge CB2 1EW, United Kingdom*
(Received 4 May 2004; published 21 September 2004)

We study the influence of shear flow on the formation of rings in a generic reversible polymer (FENE-C) model, representative for wormlike micelles. Under equilibrium conditions, rings are dominating in dilute solutions, while linear chains are dominating in strongly overlapping and concentrated solutions. We find that shear flow induces a net shift of micellar mass from linear chains to rings. At the same time, the average aggregation size of linear chains is decreasing, while the average aggregation size of rings is increasing. We hypothesize that the increased abundance and size of rings are caused by a decreased entropy gain associated with ring opening under shear flow. Linear chains and rings are elongated in the flow direction and contracted in the gradient direction. This leaves an essentially two-dimensional free volume, which two newly created chain ends can explore after being disconnected. We study the ratio of ring and linear chain distribution functions to substantiate this hypothesis. Finally, we study the rheology and discuss how the observed increase of ring abundance can provide a positive feedback between strain and ring connectivity. Such a positive feedback can contribute to shear thickening behavior, observed in micellar solutions near the overlap concentration.

DOI: 10.1103/PhysRevE.70.031502 PACS number(s): 83.80.Qr, 83.60.Rs, 82.20.Wt

I. INTRODUCTION

Surfactant molecules in solution are known to spontaneously assemble into complex structures [1]. Among these are elongated cylindrical assemblies of such great length as to be flexible and coil-like. The equilibrium statistics and dynamics of these so-called wormlike micelles resemble those of a polymer solution [2]. However, contrary to classical polymers for which the size distribution is fixed at the time of synthesis, a micellar chain can break spontaneously anywhere along the chain and recombine with other micelles, making them a part of the more general class of reversible polymers.

Recent results indicate that besides linear wormlike micelles, in *some* cases large rings may be present as well [3–5]. Rings are expected theoretically [6] for high enough values of the binding energy ("scission energy"). An important parameter, controlling the balance between linear chains and rings, is the micellar concentration. For concentrations where the wormlike micelles strongly overlap, linear chains are expected to dominate, while in dilute solutions, rings may become more important. Indeed, experimental observations of shear thickening in wormlike micellar solutions near the (apparent) overlap concentration [4,7] can be explained by assuming the presence of rings. In such systems, at low shear rates the viscosity is barely perturbed from its zero-shear value. However, above a critical shear rate the viscosity suddenly jumps to a much higher value. Cates and Candau [3] proposed a scenario in which the interlinking and delinking of large micellar rings controls this shear thickening process. Their scenario required a positive feedback between stress or strain and ring interlinking. It remained unclear, however, what the precise mechanism of the feedback would be.

The aim of this paper is to investigate the influence of shear flow on ring formation in a micellar solution. We will show that the shear flow induces an increase in the size and abundance of micellar rings, thus providing one possible positive feedback mechanism.

Our results will be obtained by means of computer simulations. There are many levels of detail with which computer simulations can be performed. Molecular dynamics simulations in full atomic detail [8] require a large number of atoms and a powerful computer. Many simulations therefore resort to coarse-grained models in which a molecule is represented by a small number of beads [9,10]. These coarse-grained models usually focus on static properties of a (part of a) single wormlike micelle, such as the bending rigidity and elastic modulus. In order to study the properties of an *ensemble* of wormlike micelles, such as the aggregate size distribution or the rheology, a much larger speedup is needed. Measurement of such properties will require simulations of very large systems on very large time scales. This can only be achieved by representing entire wormlike micelles as single chains of beads (at the cost, of course, of losing detailed information about the amphiphiles). The results we will present here are obtained from simulations of a generic model of the latter kind. In this so-called FENE-C model [11], the wormlike micelles are represented by flexible chains of relatively hard spheres. Chains can grow by the addition of monomers at the chain ends, or by recombination with other chain ends. Conversely, chains can break if any of the bonds are stretched because of thermal fluctuations or tension. The FENE-C model was studied extensively by

*Email address: jtp26@cam.ac.uk
†Email address: boek@cambridge.oilfield.slb.com

 ©2004 The American Physical Society

Kröger and others [11–14]. Usually, in these studies ring closure was explicitly disallowed. In this work, we will relax the no-loop constraint and discuss systems where linear chains have to compete with rings for the available monomers. Note that a similar approach has been taken by Kröger in Ref. [13].

This paper is organized as follows. In Sec. II we present the simulation model. In Sec. III we briefly present results and theoretical predictions for the aggregate size distribution of linear chains and rings under *equilibrium* conditions. The main results of this paper are presented in Sec. IV, where we study the influence of *shear flow* on the distribution functions and relative abundance of linear chains and rings. We summarize the results in the form of a nonequilibrium diagram of states. Next, we present a hypothesis with which we are able to explain the observed results. We study the ratio of ring and linear chain distribution functions to substantiate this hypothesis. In Sec. V we study the rheology of this model. Finally, in Sec. VI we discuss the results and describe how the observed increase of ring abundance can provide a positive feedback between strain and ring connectivity.

II. METHOD

We perform nonequilibrium molecular dynamics (NEMD) simulations of wormlike micelles in a good solvent under simple shear flow. The solution is modeled [11] by N particles which interact via two-body potentials. A fraction ϕ of these particles (the "M particles") is allowed to form wormlike chains or rings, while the remaining fraction $(1-\phi)$ (the "S particles") acts as solvent. All particles have the same mass m and the same excluded volume interactions represented by the purely repulsive part of the Lennard-Jones (LJ) potential

$$U_{ij}^{\mathrm{LJ}} = \begin{cases} 4\epsilon\left[(r_{ij}^*)^{-12} - (r_{ij}^*)^{-6} + \frac{1}{4}\right] & \text{for } r_{ij}^* \leqslant r_{\mathrm{cut}} = 2^{1/6} \approx 1.12 \\ 0 & \text{for } r_{ij}^* > r_{\mathrm{cut}} \end{cases}, \tag{1}$$

where $r_{ij}^* = r_{ij}/\sigma$ is the dimensionless distance between particles i and j. Here, and in the following, all quantities will be given in dimensionless Lennard-Jones units of length, energy, and mass (σ, ϵ, and m). Other units are derived from this, e.g., unit of time is $\sigma\sqrt{m/\epsilon}$ and unit of viscosity is $\sqrt{m\epsilon}/\sigma^2$. All M particles are able to form transient bonds with all other M particles, but every M particle can have at maximum two bonds at the same time. This condition ensures that no branched structures can occur. Supplementary to previous work by Kröger and Makhloufi [11], we allow for closed loops (of minimum size $L_c = 3$) to be formed. Two bonded M particles interact via $U^{\mathrm{bond}} = U^{\mathrm{LJ}} + U^{\mathrm{FENE-C}}$, where the FENE-C potential is given by

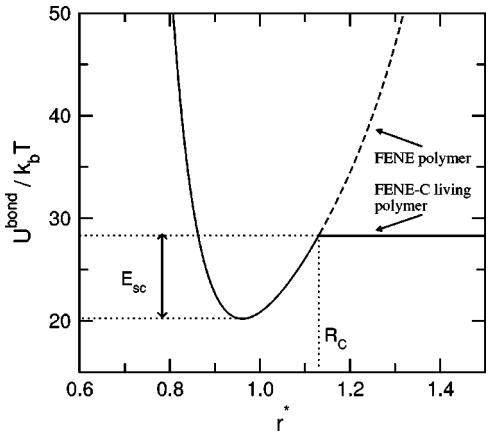

FIG. 1. Potential U^{bond} between bonded particles. The energy E_{sc} required to break a bond is set by the cutoff radius for scission R_C. This plot shows the case for which $R_C = 1.13$ and $E_{\mathrm{sc}} = 8.09\ k_BT$.

$$U_{ij}^{\mathrm{FENE-C}} = \begin{cases} -\frac{1}{2}k * R_0^2 \ln[1 - (r_{ij}^*/R_0)^2] & \text{for } r_{ij}^* \leqslant R_C \\ -\frac{1}{2}k * R_0^2 \ln[1 - (R_C/R_0)^2] & \text{for } r_{ij}^* > R_C \end{cases}, \tag{2}$$

with parameters R_0 (introducing anharmonicity), R_C (cutoff radius for scission), and k^* (spring constant). The scission energy is defined as $E_{\mathrm{sc}} = U^{\mathrm{bond}}(r^* \to \infty) - U_{\mathrm{min}}^{\mathrm{bond}}$, where $U_{\mathrm{min}}^{\mathrm{bond}}$ is the value of the potential at its minimum and $U^{\mathrm{bond}}(r^* \to \infty)$ is controlled by the cutoff radius R_C (see Fig. 1). A scission is favored for a bond that is stretched because of thermal fluctuations, or because of forces due to shear flow or entanglements. Recombination depends mainly on the fluctuations and (instantaneous) density of open ends. To compare directly with results of previous simulations of this model [11,12], we choose $R_0 = 1.5$ and $k^* = 30$. All systems contain $N = 8400$ particles, and simulations are performed at constant temperature $T^* = 1$ and particle density $n^* = 0.84$, using a conservative time step of $\Delta t^* = 0.003$. The particles undergo planar shear flow by application of Lees-Edwards boundary conditions [15], where the temperature is constrained by a Gaussian thermostat [16]. The micellar concentration ϕ is varied between 0.04 and 1, and the cutoff radius R_C is varied between 1.07 and 1.13, corresponding to scission energies E_{sc} from 3.79 to 8.09 k_BT. The latter value, at $\phi = 1$, corresponds to a chain length which is the upper limit for our system size chosen. All systems are equilibrated sufficiently long, $T_{\mathrm{eq}}^* = 5 \times 10^4$, after which measurements are taken for another $T_{\mathrm{run}}^* = 5 \times 10^4$.

III. LINEAR CHAINS AND CLOSED LOOPS IN EQUILIBRIUM

The *equilibrium* size distribution functions of self-assembled linear chains and rings have been studied extensively by Wittmer *et al.* [17] by means of different Monte Carlo methods. Our molecular dynamics results are in good

agreement with their findings. Therefore, in this section, we will focus on the theoretical predictions for the size distributions. This will be useful when interpreting the nonequilibrium results in the next section.

Wittmer *et al.* [17] expressed the free energy of the system as a simple sum over the different aggregation sizes and different species ($i=0$ for the rings and $i=1$ for linear chains). In units of k_BT,

$$F[c_0(L),c_1(L)] = \sum_{i=0}^{1}\sum_{L=1}^{\infty} c_i(L)\{\ln[c_i(L)b^3] + \mu L + \tilde{f}_i(L,\phi,E)\}. \tag{3}$$

The factor b enters for dimensional reasons and is of the order of the effective bond length. The first term is the usual translational entropy. The second term represents a Lagrange multiplier, or chemical potential μ, which fixes the total micellar concentration $\phi=\phi_0+\phi_1$. All contributions to the free energy, which are extensive or linear in L, are absorbed in this Lagrange multiplier. The terms $\tilde{f}_i$ describe the free-energy contributions not extensive in L. In general, these may depend on the interactions between different chains and may therefore differ in the dilute, semidilute, and melt regimes. The key assumption of the theory is that the distribution functions of linear chains and rings are only coupled via μ. Functionally minimizing Eq. (3), one finds

$$b^3c_0(L) = \exp[-f_0(L,\phi) - \mu L]H(L-L_c), \tag{4a}$$

$$b^3c_1(L) = \exp[-f_1(L,\phi) - \mu L - E], \tag{4b}$$

where $\tilde{f}_0+1=f_0(L,\phi)$ and $\tilde{f}_1+1=f_1(L,\phi)+E$. The free energy associated with the linear chains is split into an end-cap free energy E, which is of the order of (but not necessarily equal [17] to) the scission energy E_{sc} defined in our model, and a remaining part that describes excluded volume correlations. The Heaviside function $H(x)$ enforces a smallest possible ring size L_c, in effect a lower cutoff. In actual systems this cutoff may depend on factors, such as the detailed chemistry of the amphiphiles, and on the bending rigidity of the micelle.

A. Linear chains

Equations (4) become useful when expressions for the free energy of linear chains and rings are inserted. For dilute linear chains the free energy of a chain is given by [18] $f_1=-(\gamma-1)\ln(L)$, where $\gamma\approx1.158$ is the critical exponent for self-avoiding walks [19]. This leads to a Schultz-Zimm distribution for the linear chains,

$$b^3c_1(L) = L^{\gamma-1}\exp(-E-\mu L)\ \text{(dilute)}, \tag{5}$$

where $\mu=\gamma/\langle L_1\rangle$ [17]. This result is only valid for dilute chains, i.e., chains which are too short to overlap. Above the overlap concentration, a chain is an expanded coil until it interacts with other chains, after which the excluded volume interactions become screened. The unit of chain which is swollen is called a blob [18,20]. We define g as the number of monomers contained in one blob, and $\xi(\phi)=b_{g1}g^{\nu}$ is the blob size. Here b_{g1} relates the radius of gyration of a chain to the number of monomers, $R_g(L)=b_{g1}L^{\nu}$, where $\nu=0.588$ is the self-avoiding walk exponent. The blob size depends on the concentration, and can be estimated by using the classical definition for the crossover density of a monodisperse solution [17,20]: $4\pi/3\xi^3n\phi=g$ ($n\phi$ is the monomer number density). Using $b_{g1}\approx0.5\sigma$ [21], and $n=0.84\sigma^{-3}$, we estimate $g(\phi)\approx2.9\phi^{-1.31}$. Estimated blob sizes g for the concentrations studied here are given in Table I. For linear chains much larger than the blob size, $L\gg g$, the free energy levels off to $f_1=-(\gamma-1)\ln[g_1(\phi)]$, where $g_1(\phi)\propto g(\phi)$. This leads to an exponential distribution for the linear chains

$$b^3c_1(L) = [g_1(\phi)]^{\gamma-1}\exp(-E-\mu L)\ \text{(semidilute)}, \tag{6}$$

where $\mu=1/\langle L_1\rangle$. For concentrated solutions and melts, the blob description breaks down and the concentration dependence becomes more complicated. However, the linear-chain length distribution remains exponential [17].

TABLE I. Equilibrium properties of the $E_{sc}=8.09\ k_BT$ samples. ϕ is the fraction of M particles, ϕ_i are the fractions contained in rings ($i=0$) and linear chains ($i=1$), respectively, g is the estimated number of particles in a blob (see text), and $\langle L_i\rangle$ are the average aggregate numbers.

ϕ	g	$\langle L\rangle$	ϕ_0	$\langle L_0\rangle$	ϕ_1	$\langle L_1\rangle$
0.04	196	4.0	0.038	3.8	0.0024	7.5
0.08	79	5.9	0.067	4.1	0.013	14.9
0.16	32	20.0	0.081	4.5	0.079	35.7
0.32	13	48.9	0.085	4.7	0.235	64.9
1.00	3	128.1	0.092	5.6	0.908	140.5

B. Closed loops

The size distribution of rings is very different from that of the linear chains, and much more singular. This can be understood from a simple argument due to Porte [1,17]. The ratio of the linear chain and ring distribution functions must be equal to the ratio of the respective partition functions, which in turn must be proportional to the probability of opening a ring. The probability of opening a ring is proportional to (i) the Boltzmann weight $\exp(-E-f_1)$ to break a single bond, (ii) the number of places where the ring can break, L, and (iii) the volume R_{e1}^3 that two neighboring segments can explore after being disconnected. Hence, using Eqs. (4),

$$b^3c_0(L) = \lambda_0\frac{\exp(-\mu L)}{L[R_{e1}(L,\phi)b^{-1}]^3}H(L-L_c), \tag{7}$$

with λ_0 an unknown constant of proportionality. In the generalized case of D dimensional space, the volume that two neighboring segments can explore is given by $R_{e1}^D=b^DL^{D\nu}$. Therefore, in equilibrium, we get the following result for the distribution of rings:

$$c_0(L) \propto \exp(-\mu L)L^{-1-D\nu}H(L-L_c). \tag{8}$$

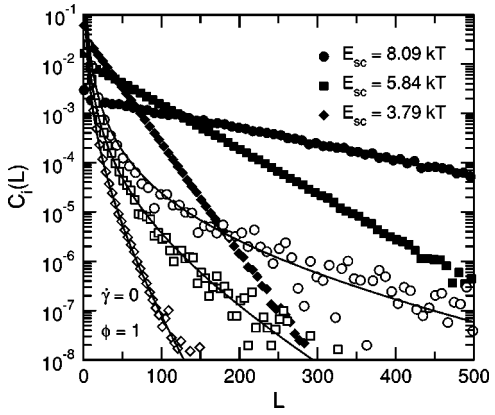

FIG. 2. Equilibrium size distribution functions under melt conditions ($\phi=1$) at various scission energies E_{sc}. Filled symbols are the distribution functions of linear chains, open symbols are the distribution functions of rings. Solid lines are theoretical predictions for the rings, Eq. (8), using $D=3$ and $\nu=1/2$.

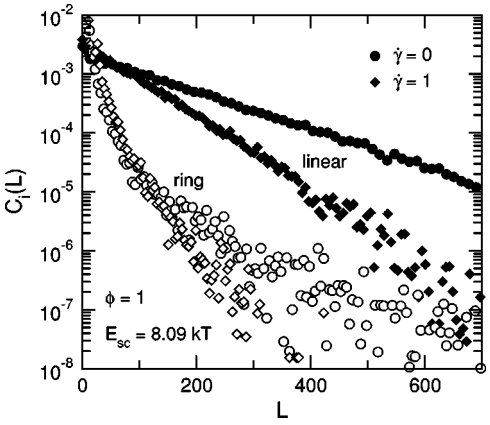

FIG. 3. Comparison of equilibrium and nonequilibrium size distribution functions for $\phi=1$ and $E_{sc}=8.09\ k_BT$. Circles are the equilibrium length distributions of linear chains (filled circles) and rings (open circles). Diamonds are the length distributions of linear chains (filled diamonds) and rings (open diamonds) under shear flow.

As a typical example, in Fig. 2 we show the equilibrium size distribution under melt conditions ($\phi=1$) at various scission energies. As expected, the length distribution of linear chains is essentially exponential (solid symbols) and the average linear length $\langle L_1\rangle$ increases rapidly with increasing scission energy and concentration (see Table I, where we also report estimated blob sizes g). The size distributions of rings are strongly singular (open symbols) and are well described by Eq. (8), with $1+D\nu=2.5$ and $\mu=1/\langle L_1\rangle$ (bold lines). Likewise in the dilute regime, both ring and linear chain distribution functions are in agreement with Eqs. (5) and (8), using $\gamma=1.158$, $1+D\nu=2.76$, and $\mu=\gamma/\langle L_1\rangle$ (not shown).

IV. LINEAR CHAINS AND CLOSED LOOPS UNDER SHEAR FLOW

In this section we will study the influence of *shear flow* on the distribution, average size, and abundance of linear chains and rings.

A. Distribution and average size

In Fig. 3 we compare equilibrium ($\dot{\gamma}=0$) and sheared ($\dot{\gamma}=1$) size distributions for $\phi=1$ and $E_{sc}=8.09\ k_BT$. Under shear flow, the probability of encountering a linear chain of a particular size decreases, relative to that probability in the quiescent state, for all chain sizes except for very small chains. Also, the average linear-chain size decreases with increasing shear rate, in agreement with previous observations in simulations of wormlike micelles [11,12]. Interestingly, the probability to encounter a ring of a particular size is found to *increase* for a wide range of ring sizes, from the smallest rings allowed (L_c) up to relatively large rings of order 100 monomers (which is much larger than the average ring size). As a result the average ring size has increased.

In Fig. 4 we take a more detailed look at how the average size of rings ($\langle L_0\rangle$) and linear chains ($\langle L_1\rangle$) varies with shear rate and concentration. We find that the average linear-chain length is decreasing with shear rate for all shear rates and all concentrations studied. At high shear rates the chains increasingly align themselves with the shear flow in order to reduce tension. However, after this reduction, an additional tension (compared to equilibrium) remains in the bonds, associated with a larger momentum transfer. This leads to the observed decrease of the average length of linear chains [12]. The dependence of the average *ring* size on shear rate is quite different. Surprisingly, for concentrations around and higher than the overlap concentration the average ring size first decreases, but then displays an upturn at the higher shear rates (in this work we define the overlap concentration ϕ^* as the concentration where the average aggregation size is equal to the blob size, $\langle L\rangle=g$, which yields $\phi^*\approx 0.20$ for $E_{sc}=8.09\ k_BT$). Before trying to explain this upturn, we will study the relative amounts of rings and linear chains.

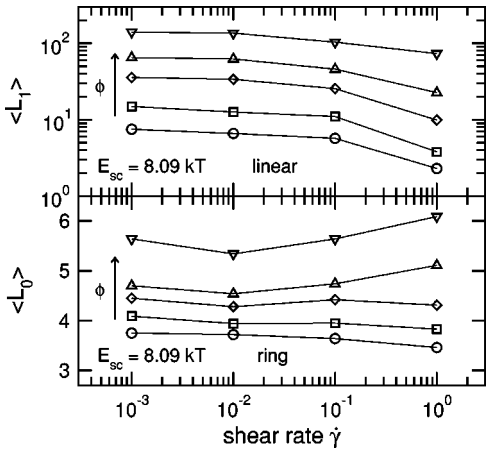

FIG. 4. Average aggregation size of linear chains (top figure) and rings (bottom figure) of the FENE-C model as a function of shear rate. The lines connect points of equal total concentration (legend in Fig. 5).

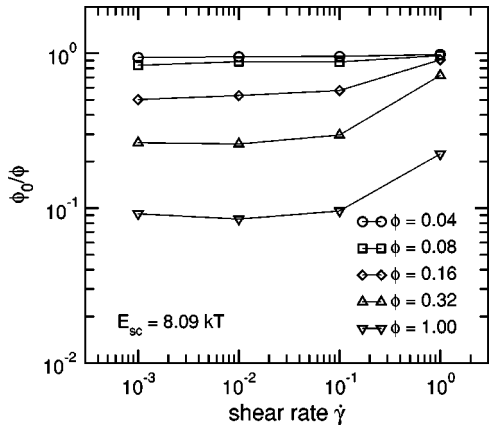

FIG. 5. Fraction of the total micellar mass contained in rings, ϕ_0/ϕ as a function of shear rate. The lines connect points of equal total concentration.

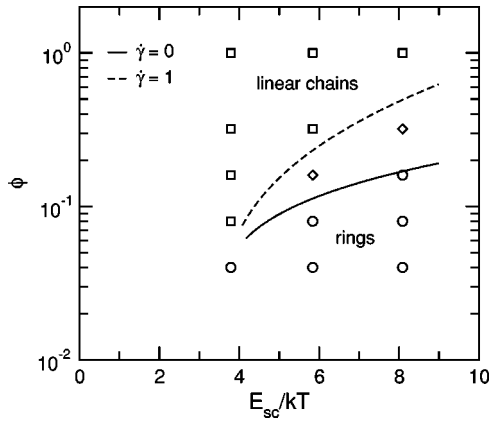

FIG. 6. A nonequilibrium diagram of states for the FENE-C model. Indicated are regimes where: (squares) linear chains are dominating at all shear rates, (circles) rings are dominating at all shear rates, and (diamonds) linear chains are dominating at low shear rates, but rings are dominating at high shear rates. The solid line is the crossover from the ring-dominated to the linear-chain–dominated regime in equilibrium. The crossover shifts to higher concentrations with increasing shear rate (dashed line).

B. Abundance of closed loops: a nonequilibrium diagram of states

In equilibrium, the abundance of rings in our model system depends on both the scission energy E_{sc} and the concentration ϕ. Let us make clear from the onset that the relative amount of rings and linear chains is much influenced by the small L behavior of rings. Because most of the ring mass is concentrated in the smallest rings, our results generally depend on the chosen cutoff L_c. Indeed, many real-life wormlike micelles have a relatively high persistence length, corresponding to a large value for L_c. However, we expect that a change in L_c will only shift the results, leaving the qualitative picture unchanged.

In Fig. 5 we present the fraction ϕ_0/ϕ of the total micellar mass contained in rings as a function of shear rate for different concentrations. In equilibrium, or at very low shear rates, going from low concentration ($\phi \ll \phi^*$) to high concentration ($\phi \gg \phi^*$), we observe a crossover from a ring-dominated system, via a system in which rings and linear chains coexist, to a linear-chain-dominated system. This can be understood from a thermodynamic argument along the lines of Eqs. (4) [17], or from a rough kinetic argument. Under dilute conditions the average distance between micellar chains and rings is large compared to the average size of a micellar chain or ring. Therefore, once a ring has opened, it is not very likely that it is in the neighborhood of another linear chain. In addition, in the dilute regime the average chain and ring sizes are small, so the amount of (additional) volume that two newly created chain ends can explore after being disconnected is relatively small. Therefore, if the scission energy E_{sc} is large enough, most of the time the two newly created chain ends will recombine with one another, promoting the presence of rings. On the other hand, in concentrated solutions there is much overlap between linear chains and rings. Therefore, once a ring has opened, it is very likely that it will recombine with another linear chain. In addition, the average chain sizes are large, so two chain ends can explore a large volume. This promotes the presence of linear chains. At the overlap concentration there is a balance between the above effects, and linear chains and rings are equally important. Indeed, at the concentration $\phi = 0.16$, which is close to our estimated overlap concentration $\phi^* = 0.20$, we find $\phi_0/\phi \approx 0.5$ (Table I).

However, it is not ruled out that shear flow may influence this balance. Indeed, Fig. 5 shows that the fraction ϕ_0/ϕ is increasing with shear rate. Since the total micellar mass is conserved, the shear flow induces a shift of mass from linear chains toward rings. This is true for all concentrations, but because rings are already dominating in the dilute systems, the effect is most clear for semidilute and concentrated systems.

More generally, we find that the abundance of rings in our model system depends on three parameters: the concentration ϕ, the scission energy E_{sc}, and, as we have seen, the shear rate $\dot{\gamma}$. In Fig. 6 we present our simulation results for three scission energies and five concentrations in the form of a diagram of states. We distinguish between regimes where rings dominate and regimes where linear chains dominate. We define the crossover to the ring-dominated regime by the equality $\phi_0 = \phi_1 = \phi/2$. Configurations with ring dominance are denoted by circles, systems where linear chains dominate by squares. The diamonds denote systems where linear chains dominate in quiescent conditions, but where rings dominate under rapid shear flow. The solid line is our estimate (by interpolation from the surrounding data) for the crossover to the ring-dominated regime in equilibrium and the dashed line is our estimate for the crossover to the ring-dominated regime for $\dot{\gamma} = 1$. Our equilibrium result is qualitatively similar to the one reported by Wittmer *et al.* [17] . These authors have also studied systems of much higher scission energies (which we were unable to do because of our limited system size). For systems containing both linear chains and rings, they showed that both the crossover concentration (as defined by $\phi_0 = \phi_1 = \phi/2$) and the overlap concentration ϕ^* (as defined by $g(\phi^*) = \langle L \rangle$) reach a plateau at high scission energies, the former lying slightly below the latter.

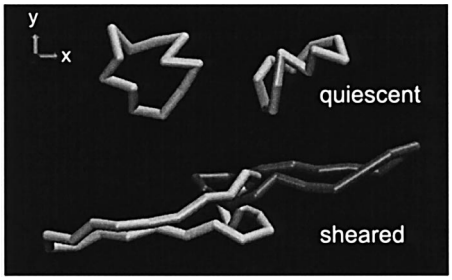

FIG. 7. Snapshots of ring configurations in equilibrium (top) and under rapid shear flow ($\dot{\gamma}=0.1$, bottom).

Now, under shear flow (dashed line in Fig. 6) we find that the crossover shifts to much higher concentrations, well within the overlap regime. Moreover, the shift is larger for larger scission energies. In the next section we will try to explain the observed effects of shear flow.

C. Hypothesis: shear-induced confinement of rings and chains to two dimensions

We will put forward a possible reason for the increase of the fraction of rings and the average size of rings under shear flow. Under rapid shear flow, the chains are stretched toward the flow direction, while contracting in the gradient direction. They maintain their equilibrium size, or contract only slightly, in the vorticity direction. This is true for rings as well (see Fig. 7). Note that the entropy of a stretched linear chain or ring is lower than that of the equivalent chain or ring in equilibrium [20]. More importantly, also the entropy gain associated with opening a ring will decrease in going from a quiescent system to a sheared one. This may be understood from the fact that the entropy gain is proportional to the logarithm of the ratio of the number of possible conformations for a linear chain and a ring. In equilibrium, the two chain ends explore a three-dimensional volume. Under rapid shear, however, we hypothesize that the two chain ends explore an essentially two-dimensional volume. The decreased entropy gain will shift the balance in favor of ring formation.

Whether or not a chain will explore an essentially two-dimensional volume will depend on its size and on the shear rate. In general, shear flow will start to affect the conformational properties of a chain of size L when the shear rate becomes larger than the inverse largest relaxation time $\tau_{\max}^{-1}(L)$ of that chain. Because wormlike micellar systems are very polydisperse, and because larger rings and chains generally have larger relaxation times, and vice versa, we expect that under shear flow there will always be a mixture of three-dimensional and two-dimensional rings and chains. In fact, the two-dimensional behavior starts only for those aggregates for which $\tau_{\max}(L)$ is much larger than the inverse shear rate in order for strong contractions in the gradient direction to occur.

To test the above hypothesis, we calculate the ratio of ring and linear-chain distributions against the aggregation number L. According to Eqs. (4) and (8), using $f_1=-(\gamma-1)\ln(L)$, we expect

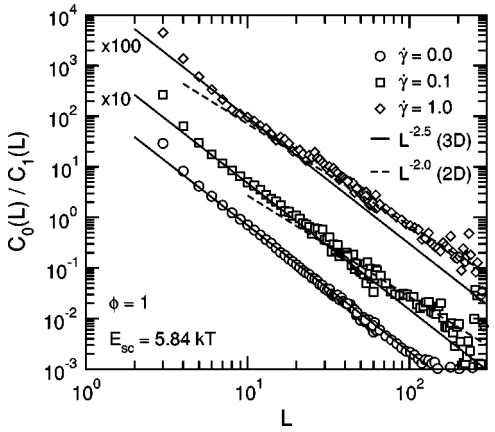

FIG. 8. Power-law behavior of the ratio of the length distributions for rings and linear chains, c_0/c_1, vs the aggregation number L in the melt. In equilibrium, the slope conforms to a power-law exponent −2.5, as expected for three-dimensional (3D) rings and chains in the melt. Under shear flow, the slope conforms to a power-law exponent −2.0 for the larger rings and chains, indicating two-dimensional (2D) behavior (data vertically shifted). The transition point from 3D to 2D behavior decreases with increasing shear rate.

$$\frac{c_0(L)}{c_1(L)} \propto L^{-\gamma-D\nu}H(L-L_c). \tag{9}$$

So, by investigating the power-law behavior of $c_0(L)/c_1(L)$, we will be able to discriminate between $D=3$ and $D=2$ rings. In the strong overlap and melt limit ($\gamma=1$, $\nu=1/2$), we expect the exponents to change from −2.5 ($D=3$) to −2.0 ($D=2$). Under dilute conditions ($\gamma=1.158$, $\nu=0.588$), we expect the exponents to change from −2.92 ($D=3$) to −2.33 ($D=2$).

In Fig. 8 we investigate the melt limit. We plot the ratio for equilibrium conditions as well as two different shear rates. The equilibrium data confirm the expected slope of −2.5 for $D=3$. In the two nonequilibrium results we recognize a transition from a slope of −2.5 for small rings and chains to a slope close to −2.0 ($D=2$) for larger rings and chains. The aggregate size L_t, where the transition occurs, decreases from $L_t\approx 40$ at $\dot{\gamma}=0.1$ to $L_t\approx 15$ at $\dot{\gamma}=1$. The decrease with shear rate is in agreement with our expectations.

Next, we investigate the dilute limit. In this limit, the fraction of mass in linear chains is very low. Unfortunately, because the linear–chain distribution occurs in the denominator of the ratio c_0/c_1, the noise also becomes relatively large in the dilute limit. In Fig. 9 we plot the ratio for equilibrium conditions and two different shear rates, and all of them for three different concentrations ϕ. Note that overlap effects become apparent only when chains are much larger than the blob size g. Therefore the largest concentration $\phi=0.16$ can still be used to investigate the dilute scaling behavior of the ratio c_0/c_1, at least up to $L\approx 100$. Indeed, the equilibrium data confirm the expected slope of −2.92 for $D=3$ for all concentrations up to and including $\phi=0.16$. The data of all concentrations coincide because the free-energy difference between rings and linear chains is independent of concentration in the dilute limit. If we now apply shear, we

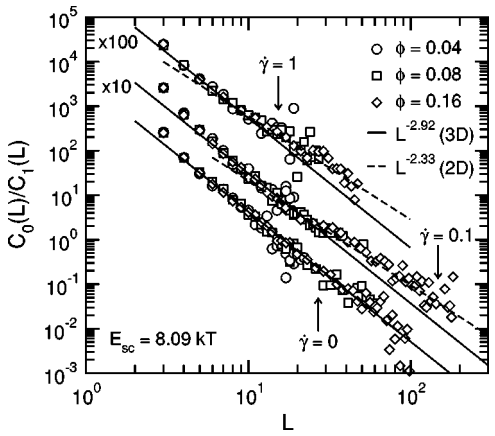

FIG. 9. Power-law behavior of the ratio of the length distributions for rings and linear chains, c_0/c_1, vs the aggregation number L for three different dilute concentrations. In equilibrium, the slope conforms to a power-law exponent −2.92, as expected for dilute 3D rings and chains. Under shear flow, the slope conforms to a power-law exponent −2.33 for the larger rings and chains, indicating 2D behavior (data vertically shifted). The transition point from 3D to 2D behavior decreases with increasing shear rate.

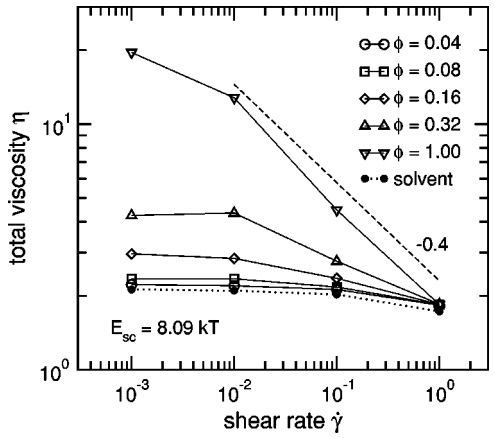

FIG. 10. Total shear viscosity η of the FENE-C model as a function of shear rate (open symbols). The shear viscosity of the pure solvent ($\phi=0$, closed circles) is also given.

recognize a transition to a slope close to −2.33 ($D=2$) for the larger rings and chains, again consistent with our hypothesis.

These observations confirm our hypothesis that shear flow causes a fraction of the system to behave like two-dimensional rings and chains. This causes rings to become more abundant and the average ring size to increase at high enough shear rates. Moreover, at a given shear rate $\dot\gamma$ and concentration ϕ, the effect will become larger for systems with higher scission energies E_{sc}, because such systems have larger average ring and chain sizes already in equilibrium.

The observed effects of shear may enhance the shear thickening observed in real-life micellar systems with high enough scission energy and concentrations around or slightly below the overlap concentration [3,4]. In the next section we will therefore pay some attention to the rheology of our model system. We will return to real-life micellar systems in the Discussion.

V. RHEOLOGY

In many applications, wormlike micelles are used as rheology control agents. As a consequence, much of the characterization of wormlike micellar solutions is done by means of rheometry. In a molecular dynamics simulation, the rheology can be determined by measuring the instantaneous stress tensor. Its components are given by [20]

$$\sigma_{\alpha\beta} = -\frac{1}{V}\left(\sum_{i=1}^{N} m v_{i\alpha} v_{j\beta} + \sum_{i=1}^{N-1}\sum_{j=i+1}^{N} r_{ij\alpha} F_{ij\beta}\right). \qquad (10)$$

Here $v_{i\alpha}$ is the α component of the velocity of particle i, $r_{ij\alpha}$ the α component of the vector from the position of particle j to particle i, and $F_{ij\beta}$ the β component of the force exerted by particle j on particle i (we have assumed a pairwise interacting system). The shear viscosity η of a system undergoing planar shear flow in the x direction, with the gradient in the y direction, can be determined from the time-averaged xy component of the steady–state shear stress,

$$\eta = \frac{\langle \sigma_{xy} \rangle}{\dot\gamma}. \qquad (11)$$

In Fig. 10 we plot the measured shear viscosity versus shear rate for $E_{sc}=8.09\ k_BT$ at five different concentrations. The system displays shear thinning behavior at all concentrations. The shear thinning reaches a slope of −0.4 (dashed line) for the highest concentration $\phi=1$. At low shear rates, the viscosity levels off to a constant value, which is the zero-shear viscosity. Within the range of shear rates studied, this plateau is reached for all concentrations but the highest. In Fig. 10 we have also plotted the shear viscosity of the pure solvent ($\phi=0$, dotted line). We confirm that at low concentrations (or all concentrations at high enough shear rate) the viscosity approaches that of the solvent.

The observed shear thinning behavior is reminiscent of experimental observations in wormlike micelles. However, in experiments the shear thinning of the viscosity is much stronger, with a slope as low as −1 for strongly overlapping wormlike micelles. This now exposes an important difference between experimental wormlike micelles and the current FENE-C model. In experimental semidilute and concentrated systems, the shear stress in equilibrium is dominated by contributions from the temporary network (or matrix) formed by the micelles. In other words, the solvent (usually water) does not contribute significantly to the zero-shear viscosity. Under rapid shear flow, the network becomes strongly aligned, resulting in excessive shear thinning until the viscosity of the solvent is reached. On the other hand, in the FENE-C model, excluded volume interactions between solvent spheres are often dominating the network contribution to the shear stress. This is caused by the fact that, unlike real solvents, the solvent particles in the FENE-C model are of the same size and rigidity as the micelle forming particles. This results in a relatively high solvent contribution to the shear viscosity.

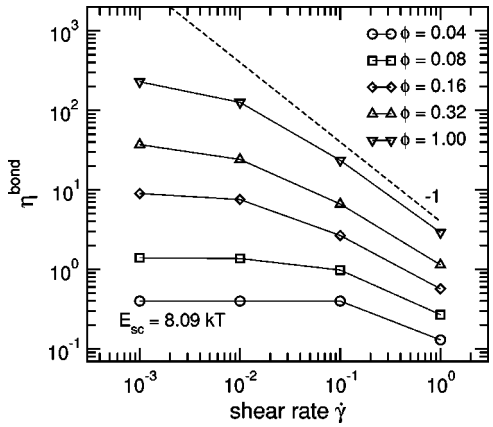

FIG. 11. Viscosity η^{bond} based on the stress through the bonds between micellar monomers.

Steeper shear thinning slopes may be observed in the FENE-C model when using higher scission energies E_{sc}. However, because the solvent contribution will always be unrealistically high, we expect that E_{sc} must become unrealistically high as well.

Let us now, for an instance, ignore the excluded volume contributions to the shear stress. In Fig. 11 we have plotted the viscosity η^{bond}, defined similar to Eq. (11) but with the stress tensor based on the bonds between micellar monomers only. Much stronger shear thinning is observed now, with a slope close to -1 (dashed line) for the highest concentration $\phi=1$, in apparent agreement with experimental observations. Note that the viscosity results for the FENE-C model (excluding ring formation) presented by Carl *et al.* [12] were calculated in a similar way, i.e., disregarding solvent contributions, although the authors did not explicitly state this. As we have seen, when solvent contributions are included, the shear thinning effects become much less dramatic.

VI. DISCUSSION AND CONCLUSIONS

We have studied the influence of shear flow on the formation of rings in wormlike micelles by means of nonequilibrium molecular dynamics simulations of the FENE-C model [11]. As we have already made clear, the results presented here depend on the smallest ring size allowed, which in reality would be determined by such factors as the chemistry of the amphiphiles and the bending rigidity of the wormlike micelles. It has been argued in the literature that rings shorter than roughly a persistence length are highly unlikely to form [1]. This might be the reason why rings seem to be unimportant in some giant micellar systems. On the other hand, closed loops have been observed (or at least their presence suggested) in other giant micellar systems [3–5] as well as other types of equilibrium polymers, such as liquid sulfur [6]. For such systems, the results we have found will be relevant, at least in a qualitative way.

For the equilibrium case, i.e., in the absence of shear flow, we have confirmed the findings of Wittmer *et al.* [17]: rings are dominating in dilute solutions, while linear chains are dominating in strongly overlapping and concentrated solutions and melts. The crossover concentration between the two regimes is close to the overlap concentration.

We have found that, as a result of shear flow, the crossover between ring and linear-chain-dominated regimes increases to higher concentrations (Fig. 6). In other words, at fixed micellar concentration the shear flow induces a net shift of micellar mass from linear chains to rings. At the same time, the average aggregation size of linear chains is decreasing with increasing shear rate, while the average aggregation size of rings is first decreasing but then increasing. We have put forward the hypothesis that this increase of ring abundance and size is caused by a decrease of entropy gain associated with ring opening under shear flow. The conformations of large chains and rings, whose typical relaxation times are much larger than the inverse shear rate, will be altered significantly by the shear flow. They will be elongated in the flow direction, and, as a result of their finite extensibility, contracted in the gradient direction. This leaves an essentially two-dimensional free volume which two newly created chain ends can explore after being disconnected. We realize that we have applied (equilibrium) statistical-mechanical arguments to nonequilibrium conditions. The relative motion of rings and chains within each layer perpendicular to the gradient direction is slow, however, and quasistatic arguments may apply. Indeed, we have been able to substantiate the hypothesis by studying the power-law behavior of the ratio $c_0(L)/c_1(L)$, which, according to Eq. (9) is sensitive to the dimensionality D of the free volume. Our results are consistent with $D=2$ for large rings and chains, although a fractal dimension cannot be excluded; a joint least-squares fit with the high-L data in Figs. 8 and 9 yields $D=2.1\pm0.3$.

On the rheological side, we have found that the viscosity is decreasing with shear rate. The shear thinning exponent, however, is less pronounced (-0.4) than expected from similar experimental wormlike micelles (-1). The failure of the model to predict the correct shear thinning behavior is attributed to the dominance of solvent excluded volume effects in the FENE-C model. We expect to observe the correct slope of -1 within the FENE-C model only when much larger values of the scission energy E_{sc} are used. In that case the chains will be much longer, the zero-shear viscosity much higher, and the critical shear rate (where shear thinning begins) much lower, leaving more "room" for shear thinning.

In experiments, wormlike micellar systems are not only observed to shear thin, but sometimes also to *shear thicken* [4]. Although this phenomenon was not observed in our simulations, we believe we have found a mechanism by which shear thickening can be explained.

Shear thickening systems are usually just below the overlap concentration and typically show a factor of 10 increase in viscosity around some critical shear rate $\dot{\gamma}_c$, while below $\dot{\gamma}_c$ the viscosity is barely perturbed from its zero-shear value η_0. As already mentioned in the Introduction, Cates and Candau [3] have put forward a speculative scenario in which large *interlinked rings* are driving this shear thickening behavior. If the linking and delinking kinetics is sufficiently slow, a percolating network of interlinked rings will indeed be able to transfer much more stress. Their scenario may also explain why shear thickening is only observed near the over-

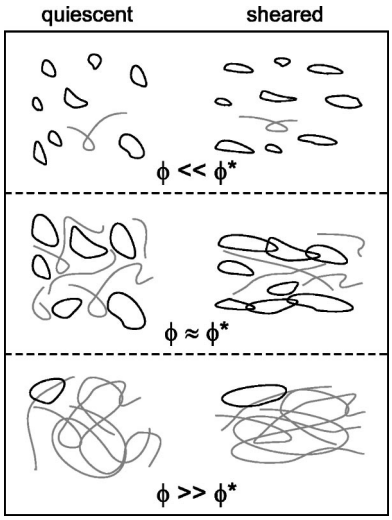

FIG. 12. Cartoon of wormlike micellar configurations in quiescent and sheared conditions. For $\phi \ll \phi^*$ (top figure) many rings are present, but they do not overlap. For $\phi \gg \phi^*$ (bottom figure) hardly any rings are present. Only near the overlap concentration (middle figure) enough rings may be present which can interlink, increasingly so, under shear flow.

lap concentration. Far below the overlap concentration the aggregates, although mainly in the form of rings, do not overlap or interlink. On the other hand, far above the overlap concentration there are hardly any rings to interlink: the aggregates are mainly in the form of linear chains which are entangled with each other. Only at (or slightly below) the overlap concentration is there a balance between rings and linear chains. (See Fig. 12 or a cartoon of the three different concentration regimes under quiescent and sheared conditions.) Cates and Candau described the possibility of a partially percolating structure of interlinked rings in the quiescent state, which becomes fully percolating as a result of shear flow. In order to explain the shear thickening effect fully, they needed a positive feedback between stress or strain and ring linking. Our work suggests that one possible positive feedback mechanism is provided by the shear-induced confinement of linear chains and rings to a lower dimensional space, leading to larger and more abundant ring aggregates. It should be noted that in this work the confinement effects become apparent only at relatively high shear rates. Experimental micellar systems usually have much higher scission energies and therefore much larger chains and rings than the ones studied here. Consequently, relaxation times are much larger and critical shear rates for nonlinear behavior are much lower. Moreover, the *largest* (rather than the average) rings will form the percolating network. This leads us to believe that, in experimental systems, confinement effects become important at much lower shear rates than the ones studied here.

In our simulations shear thickening was not observed. The root of the problem lies in the fast scission and recombination kinetics (and thus linking and delinking kinetics) of the FENE-C model. Recombination is relatively easy in this model, because chain ends can fuse instantly if their separation is smaller than R_C (Fig. 1). In reality, before two chain ends can fuse, there may be specific demands on the conformations of the amphiphiles in the end caps, giving rise to a free-energy barrier. Chain recombination, like scission, may therefore be an activated process. A typical value for the height E_a of the free-energy barrier may be estimated from experiments on EHAC wormlike micelles [22,23], yielding $E_a \approx 12.5\ k_B T$. Such a high activation barrier will substantially decrease the rate with which wormlike micelles are breaking up. As a consequence, the linking and delinking kinetics of rings in *real* wormlike micelles can be very slow, opening up the route to shear thickening behavior.

We can finally conclude that the FENE-C model has taught us a lot about the equilibrium and nonequilibrium behavior of flexible wormlike micelles. The original FENE-C model can still be motivated by the fact that the *equilibrium* distributions should be unaffected by any recombination activation barrier. However, great care must be taken if realistic and quantitative results for the *dynamics* and *rheology* of wormlike micelles are required. Currently, we are developing a model in which a significant recombination activation barrier will be incorporated, and where the solvent contribution to the stress tensor will be negligible (Brownian dynamics). Another step towards realism concerns the persistence length. Usually the persistence length of a wormlike micelle is much larger than its diameter [8]. This may be modeled by means of a bending potential between the (spherical) beads, as in Ref. [13]. Unfortunately, this quickly becomes very CPU-intensive, as many beads will be required to represent just one persistence length of a realistic wormlike micelle. We will therefore represent wormlike micelles by long and thin segments, each segment measuring an entire persistence length. We will deal with the uncrossability of such segments by means of the TWENTANGLEMENT method, details of which can be found in Ref. [24].

ACKNOWLEDGMENTS

We thank John Crawshaw for careful reading of the manuscript. J.T.P. is financially supported by a grant from the U.K. Engineering and Physical Sciences Research Council (EPSRC) through the IMPACT Faraday Partnership Programme.

[1] *Micelles, Membranes, Microemulsions, and Monolayers*, edited by W. M. Gelbart, A. Ben-Shaul, and D. Roux (Springer-Verlag, New York, 1994).
[2] M. E. Cates and S. J. Candau, J. Phys.: Condens. Matter **2**, 6869 (1990).
[3] M. E. Cates and S. J. Candau, Europhys. Lett. **55**, 887 (2001).
[4] Cl. Oelschlaeger, G. Waton, E. Buhler, S. J. Candau, and M. E. Cates, Langmuir **18**, 3076 (2002).

[5] T. M. Clausen, P. K. Vinson, J. R. Minter, H. T. Davis, Y. Talmon, and W. G. Miller, J. Phys. Chem. **96**, 474 (1992); M. In, O. Aguerre-Chariol, and R. Zana, *ibid.* **103**, 7747 (1999); A. Bernheim-Groswasser, R. Zana, and Y. Talmon, *ibid.* **104**, 4005 (2000).
[6] R. G. Petschek, P. Pfeuty, and J. C. Wheeler, Phys. Rev. A **34**, 2391 (1986).
[7] H. Rehage, I. Wunderlich, and H. Hoffmann, Prog. Colloid Polym. Sci. **72**, 11 (1997).
[8] E. S. Boek, W. K. den Otter, W. J. Briels, and D. Iakovlev, Philos. Trans. R. Soc. London, Ser. A **362**, 1625 (2004).
[9] R. Goetz and R. Lipowsky, J. Chem. Phys. **108**, 7397 (1998).
[10] W. K. den Otter, S. A. Shkulipa, and W. J. Briels, J. Chem. Phys. **119**, 2363 (2003).
[11] M. Kröger and R. Makhloufi, Phys. Rev. E **53**, 2531 (1996).
[12] W. Carl, R. Makhloufi, and M. Kröger, J. Phys. II **7**, 931 (1997).
[13] M. Kröger, Macromol. Symp. **133**, 101 (1998).
[14] M. Kröger, Phys. Rep. **390**, 453 (2004).
[15] M. P. Allen and D. J. Tildesley, *Computer Simulation of Liquids* (Clarendon, Oxford, 1987).
[16] F. Zhang, D. J. Searles, D. J. Evans, J. S. den Toom Hansen, and D. J. Isbister, J. Chem. Phys. **111**, 18 (1999).
[17] J. P. Wittmer, P. van der Schoot, A. Milchev, and J. L. Barrat, J. Chem. Phys. **113**, 6992 (2000).
[18] P. G. de Gennes, *Scaling Concepts in Polymer Physics* (Cornell University, Ithaca, New York, 1979).
[19] S. Caracciolo, M. S. Causo, and A. Pelissetto, Phys. Rev. E **57**, R1215 (1998).
[20] M. Doi and S. F. Edwards, *The Theory of Polymer Dynamics* (Clarendon, Oxford, 1986).
[21] K. Kremer and G. S. Grest, J. Chem. Phys. **92**, 5057 (1990).
[22] I. Couillet, T. Hughes, G. Maitland, F. Candau, and S. J. Candau (unpublished).
[23] J. T. Padding and E. S. Boek, Europhys. Lett. **66**, 756 (2004).
[24] J. T. Padding and W. J. Briels, J. Chem. Phys. **115**, 2846 (2001).